Astronomy & Astrophysics manuscript no. on1paper February 2, 2008
(DOI: will be inserted by hand later)

arXiv:astro-ph/0406646v1 29 Jun 2004

The structure of Onsala 1 star forming region

M. S. N. Kumar[1], M. Tafalla[2] and R. Bachiller[2]

[1] Centro de Astrofísica da Universidade do Porto, Rua das Estrelas, 7150-462 Porto, Portugal
e-mail:nanda@astro.up.pt,
[2] Observatorio Astronómico Nacional, Alfonso XII, 3, E-28014 Madrid, Spain

Received: ; accepted:

Abstract. We present new high-sensitivity high-resolution mm-wave observations of the Onsala 1 ultra-compact HII region that bring to light the internal structure of this massive star forming cloud. The 1.2 mm continuum map obtained with the IRAM 30-m radiotelescope ($\sim$11″ resolution) shows a centrally peaked condensation of 1′ size ($\sim$0.5 pc at the assumed distance of 1.8 kpc) which has been further investigated at higher resolution in the 3 mm continuum and in the emission lines of $H^{13}CO^+$ J=1–0 and SiO J=2–1 with the IRAM Plateau de Bure interferometer. The 3 mm data, with a resolution of $\sim 5'' \times 4''$, displays a unresolved continuum source at the peak of the extended 1.2 mm emission and closely associated with the ultra-compact HII region. The $H^{13}CO^+$ map traces the central condensation in good agreement with previous NH_3 maps of Zheng et al.1985. However, the velocity field of this central condensation, which was previously thought to arise in a rapidly rotating structure, is better explained in terms of the dense and compact component of a bipolar outflow. This interpretation is confirmed by SiO and CO observations of the full region. In fact, our new SiO data unveils the presence of multiple (at least 4) outflows in the region. In particular, there is an important center of outflow activity in the region at about 1′ north of the UCHII region. Indeed the different outflows are related to different members of the Onsala 1 cluster. The data presented here support a scenario in which the phases of massive star formation begin much later in the evolution of a cluster and/or UCHII region last for much longer than 10^5yrs.

Key words. Stars: formation –Interstellar medium: jets and outflows – ISM: HII regions–ISM: clouds

1. Introduction

Onsala 1 (ON 1) is an ultra-compact HII (UCHII) region situated in the densest part of the Onsala molecular cloud (Israel & Wootten 1983). It is one of the most compact and isolated UCHII regions known to be associated with several signposts of massive star formation such as dense gas, high velocity gas, masers, and near-infrared sources. However, a single luminous ($10^4.2\,L_\odot$) far-infrared (FIR) point source namely IRAS20081+3132 is associated with this UCHII region. The luminosity estimated from FIR data and the centimeter(radio) emission agree well, within a factor of $100\,L_\odot$, and indicate a spectral type of B0.3-B0.6 (MacLeod et al. 1998). At a spatial resolution of 0.7″-1.5″, the UCHII is detected as an unresolved source at 2 cm & 3 cm wavelengths (Kurtz et al.1994). Higher angular resolution(0.1″) observations at 1.2 cm resolve the UCHII region into an approximate shell structure of size 0.6″(Turner & Matthews 1984). This source is placed at a distance of 1.3-6 kpc by various authors in the literature. However, a distance of less than 2 kpc is favored by most authors for many valid reasons (see e.g. MacLeod et al.1998; Watson et al. 2003). We therefore adopt the near-distance of 1.8 kpc to this source for the purposes of this work.

Several masers such as OH (Ho et al. 1983), H_2O (Downes et al. 1979), CH_3OH (Menten 1991) and HCHO (MacLeod et al. 1998) are known to coincide with ON 1. Spatially separated blue and red shifted OH maser spots around ON 1 have been identified by Desmurs & Baudry (1998) using VLBI techniques. Observations using dense gas and dust tracers have shown a compact, nearly circular dense core surrounding ON 1. Maps of 350μm continuum emission (Mueller et al. 2000) and CS J=5-4 emission (Shirley et al. 2003) show dense circular condensations around the source. Emission from transitions of CH_3CN J=12-11 (Pankonin et al. 2001) and HNCO (Zinchenko et al. 2000) are also found to peak on ON 1. Using VLA observations at 11″resolution in the (J,K)=(1,1) line of NH_3, Zheng et al. (1985, hereafter ZHRS85) argued for the presence of a rapidly rotating gas condensation centered on ON 1. However, the regions of massive star formation often possess an intricate kinematic behavior involving motions of rotation, infall, and outflow, and the actual existence of a rapid gas condensation in ON 1 needed con-

Send offprint requests to: M. S. Nanda Kumar

firmation with higher resolution observations. In this paper, we present high-sensitivity high-resolution (∼5″) line and continuum observations which are used to investigate in detail the dense core and outflowing gas associated with ON 1.

2. Observational Data

The IRAM 30 m radiotelescope at Pico Veleta (near Granada, Spain) was used to map the λ 1.2 mm continuum emission from the ON 1 region in December 2000. We used the MAMBO 1 bolometer array to produce an on-the-fly map with a scanning speed of 4″ s^{-1}, a wobbler period of 0.5 s, and a wobbler throw of 53″. The central frequency of the detectors was ∼240 GHz, and the bandwidth ∼70 GHz. Sky dips made immediately before and after the map were used to correct for the atmospheric extinction, and a global calibration factor of 15000 counts per Jy (based on an observation of Uranus) was applied to the data. The resulting map (produced with the IRAM NIC software) has an angular resolution of 11″.

High resolution interferometric observations of ON 1 region were carried out using the IRAM Plateau de Bure (PdB) interferometer (near Grenoble, France) in its D (5 antennas) and C (6 antennas) configurations. Observations using the compact D array configuration were carried out on the nights of 28 May 2002 and 20 July 2002 for two adjacent fields; one field centered on the ON 1 FIR point source/UCHII region and another at offset 1′north. The C array configuration observations for the same fields were obtained during the nights of 9 and 10 January 2003. Each field was a mosaic of 9 pointings arranged in a 3×3 matrix with a spacing of 12″ which is roughly equal to half the primary beam size. We used the SIS heterodyne receivers both at 87 GHz and 230 GHz. The 230 GHz data was mostly unusable due to summer weather conditions. Six spectral correlators were used to select three spectral lines, namely, SiO J=2–1(ν=86.846891 GHz), $H^{13}CO^+$ J=1–0 (ν=86.754330 GHz) and CO J=2–1 (ν=230.538 GHz) and two continuum bands centered at 1.2 mm and 3 mm wavelengths. The system temperature was typically 100 K at 3 mm and >400 K at 1.2 mm with a phase noise of ∼25°-35°at 3 mm and >40°-50° at 1.2 mm. The D configuration provided baselines of 24m-82m while the C configuration resulted in baseline range of 48m-229m. We used the sources 2023+336 and 2013+370 as the primary phase calibrators and MWC349, 2013+370 and 3C345 for flux calibration. Synthesized clean beams at 3 mm measured ∼5.35″×3.7″ (PA=56°) which represent the typical resolution of the interferometric data presented here. The resulting maps does not include any short spacing data from single dish observations and thus filter out all large scale structures.

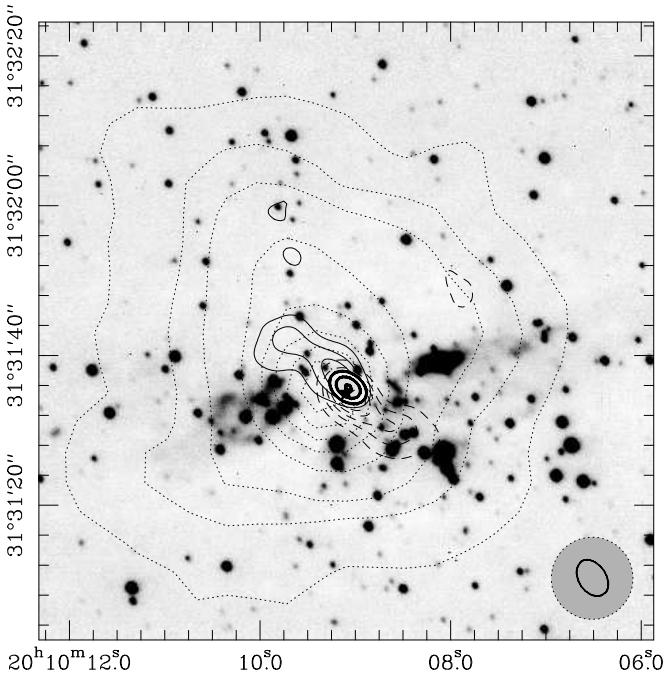

Fig. 1. 1.2 mm continuum emission (dotted contours) mapped with IRAM30 m telescope overlayed on a K-band image (Kumar et al. 2003) of the Onsala 1 region. Contour levels are 1,2,3,6,9,12,15,18 & 21 Jy/beam and has an rms of 140mJy/beam. Thick contours enclosing grey shades represent the 3 mm continuum emission mapped with the IRAM PdB interferometer. Levels are 0.1, 0.15 & 0.2 Jy/beam (rms = 1.6mJy/beam). The star symbol represents the position of the FIR sources and the UCHII region. Solid lines represent blue-shifted and dashed lines represent red-shifted $H^{13}CO^+$ J=1–0 emission, integrated in the velocity range V_{lsr}±4.5 km s^{-1}. In both cases, the contour levels start at 0.5 K km s^{-1} (rms = 0.06 Kkm s^{-1}) and increase in steps of 0.5 K km s^{-1}. The beam sizes of the 1.2mm data(dotted circle) and the 3mm data (bold ellipse) are shown enclosed in grey shades at the bottom right corner of the figure.

3. Results

3.1. Continuum observations

In Fig.1 we depict the results of observations that represent the dense gas and dust in the region of ON 1. The star symbol shows the coinciding position of the UCHII region, the luminous IRAS point source and all the maser spots that represent the massive young stellar object, which we shall henceforth refer to as ON 1. The 1.2 mm continuum emission is extended over a size scale of ∼70″ and elongated in the North-East direction. The 1.2 mm continuum emission is a sensitive tracer of the warm dust and therefore indicates the dense cloud surrounding ON 1. The spatial extent and morphology of the 1.2 mm continuum map is very similar to that of 350μm map (Mueller et al. 2000), the CS emission line maps (Shirley et al. 2003) and also the integrated NH_3 emission (ZHRS85) which has been

thought to represent a rapidly rotating condensation. The source ON 1 and the surrounding embedded cluster all appear well immersed in the observed 1.2 mm emission. Therefore the 1.2 mm emission region in Fig. 1, which is representative of the condensation unveiled by all other dense gas tracers, can be considered as the dense core in which the ON 1 cluster has been forming. The 3 mm continuum emission reveals an unresolved source centered on ON 1. The interferometric observations filter out the extended emission and show the underlying small scale structure. Therefore the 3 mm continuum emission centered on ON 1 is indicative of the major condensations within the more extended clump traced by the 1.2 mm emission. However, 10μm observations (Kumar et al. 2003) reveal two closely situated sources coinciding with the unresolved 3 mm source indicating that ON 1 is likely to harbor a binary protostar.

The 1.2 mm emission maps can be used to estimate the mass of the ON 1 clump and the 3 mm continuum emission the mass of the unresolved central source(s). The black body fits to the Far-Infrared (FIR) flux density distribution of ON 1 indicates a dust temperature of 57 K (Mueller et al. 2000). Since the peak of the dust condensation coincides with an UCHII region, this value is likely an upper limit. If we assume a dust absorption coefficient of $\kappa_{1.2mm}$=0.0005 kg^{-1}m^2 (Henning et al. 1985) and a distance of 1.8 kpc to the source, the observed 1.2 mm continuum emission represents a cloud mass of $\sim$3860M$_\odot$ for T=50K and 5000M$_\odot$ for T=40K. The source averaged flux density (3.6 Jy/beam) imply hydrogen column densities of 1.4×10^{24}cm^{-2} resulting in A$_v$ $\sim$700 mag. The peak column density is even higher at 8.2×10^{24}cm^{-2} implying a few thousand magnitudes of visual extinction. However, these numbers are to be treated with caution due to the presence of the UCHII region. The observed emission does not faithfully represent the temperature of the warm dust since the heating effects of the UCHII region can contribute to a majority of emission close to the peak. The 3 mm emission from the unresolved source represents a mass of $\sim$400M$_\odot$, where we have used κ_{3mm}=6.6×10^{-5} kg^{-1}m^2. This value of κ_{3mm} is obtained by assuming a spectral emissivity index β=2. There is increasing observational evidence which suggest that the value of β is likely much lower (β $\sim$1) around massive protostellar sources (ex: Hunter et al.2000) . If we assume β $\sim$1 then the resulting estimates of the embedded mass in the observed 3 mm emission will be lower than quoted above. In any case, the derived mass from 3 mm emission is probably an over estimate since 3 mm continuum emission is known to trace free-free emission also and may not be a good tracer of the dust alone (Downes et al. 1992). In view of these facts we can safely assume that the enclosed mass in the unresolved central object is not greater than $\sim$300-400M$_\odot$. Thus about 6-8% of the overall dense core mass seems to be in the form of protostellar material at the center.

3.2. $H^{13}CO^+$ J=1–0 Emission

In Fig. 1 solid and dashed contours show blue and red shifted $H^{13}CO^+$ J=1–0 emission, respectively, integrated in the velocity range V$_{lsr}$$\pm$4.5 km s^{-1}. As evident from the figure, the $H^{13}CO^+$ emission is centered on the source ON 1 and reveals a spatially resolved bipolar structure. The position angle (PA) of the axis of this well-collimated bipolar structure is $\sim$44° and roughly coincides with the elongation displayed by the 1.2 mm contours. The $H^{13}CO^+$ emission also coincides well with the NH_3 condensation mapped by ZHRS85. The projected length of this bipolar emission is $\sim$30″ corresponding to about 0.27 pc at the assumed distance of 1.8 kpc. Each lobe of this compact feature appears to consist of two distinct clumps.

In Fig. 2 we show a velocity-position map obtained along the axis (PA$\sim$44°) of this bipolar feature which reveals a structure that is distinctly different from earlier claims of ZHRS85. The vertical line represents the systemic LSR velocity at 12 km s^{-1}. The red-shifted southern lobe and the blue-shifted northern lobe can be seen clearly separated into two components on the PV diagram. A main component of the emission (denoted by A & B in Fig. 2) stretches to a radius of $\sim$5″ and a satellite component comprising of two knots (denoted by C & D) extends to a radius of $\sim$10″. These 4 clumps correspond to the clumps found on the images (Fig.1). As can be seen from Fig.2, all of the found emission is spread along a straight line on the PV-plane showing increasing velocity with increasing distance from the central position following a Hubble law. We have not subtracted the bright continuum emission from this data. The continuum emission can therefore be seen close to the source (offset = 0) extending on either side of the V$_{lsr}$, up to the limits of our observing setup with the spectrometers.

Since the $H^{13}CO^+$ J=1–0 emission is symmetrical both in position and velocity with respect to the central position and velocity, it is natural to conclude that such emission arises in a bipolar outflow emerging from the central object. Note that the observed kinematical structure can not be easily explained with a rotating disk. First of all, the total size of this structure (>0.2 pc) is too large to be a disk and, moreover, a disk would produce just two peaks of emission in the PV diagram, not four peaks as the A,B,C, & D peaks which are actually observed in Fig. 2. The Hubble-like velocity law distribution which is observed in Fig. 2 (velocity proportional to the distance) is also very typical of young bipolar outflows. A straight line fit through all the knots shows a gradient of $\sim$30 km s^{-1} pc^{-1} at the assumed distance of 1.8 kpc. These velocity limits and the velocity gradient are similar to the values obtained from NH_3 observations by ZHRS85 except that the gradient of $\sim$11 km s^{-1} pc^{-1} estimated by ZHRS85 is due to their adopted distance of 3.5 kpc. The interpretation that the $H^{13}CO^+$ emission arises in the compact component of a bipolar outflow is confirmed by the SiO high-velocity data shown in the following section.

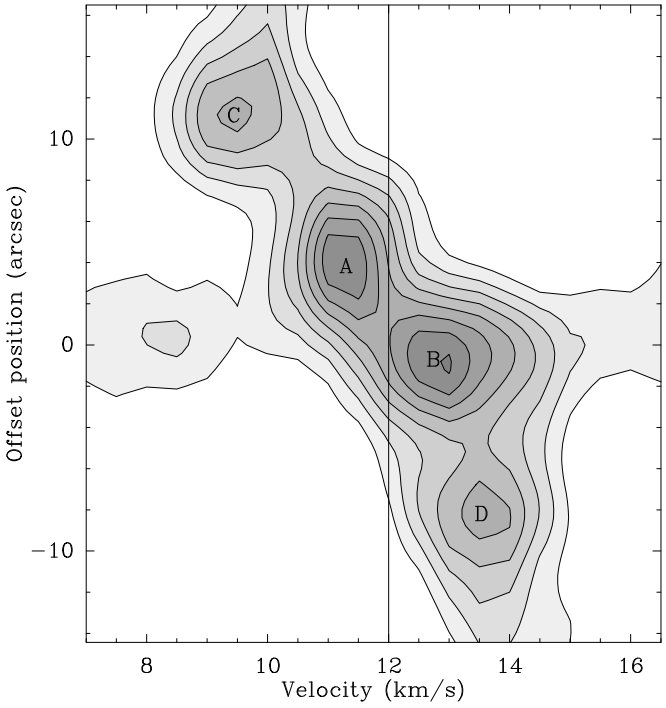

Fig. 2. Velocity-Position diagram for the $H^{13}CO^+$ J=1–0 emission shown in Fig. 1, obtained along the axis of the bipolar emission at PA∼44°. The contours levels start at 1 K and increase in steps of 1 K.

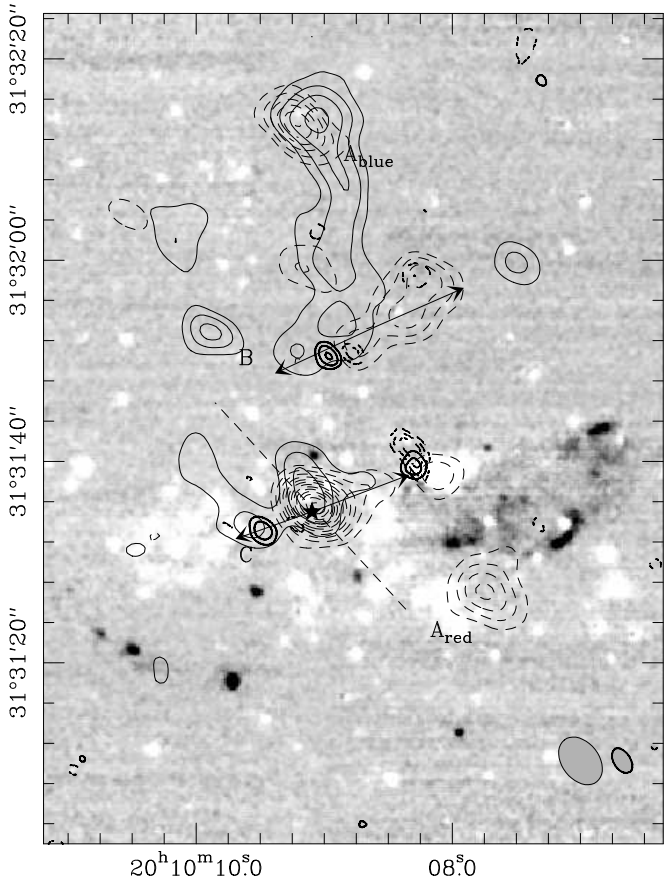

Fig. 3. SiO J=2–1 (thin lines) and CO J=2–1 (thick lines) integrated emission overlayed on a continuum subtracted H_2 narrow band image at 2.122μm. SiO emission was integrated with a velocity interval of $V_{lsr}\pm4\,km\,s^{-1}$ and CO emission was integrated in the range $V_{lsr}\pm12\,km\,s^{-1}$ Solid lines represent blue-shifted and dotted lines represent red-shifted emission. SiO contour levels start at $0.2\,K\,km\,s^{-1}$ (rms = $0.06\,Kkm\,s^{-1}$) and increase in steps of $0.15\,K\,km\,s^{-1}$. CO contours levels start at $2\,K\,km\,s^{-1}$ (rms = 0.22 K kms) and increase in steps of $1\,K\,km\,s^{-1}$. The star symbol represents the position of the FIR sources and the UCHII region as in Fig. 1. The dotted straight line represents the axis of the $H^{13}CO^+$ outflow. The beam sizes of the 3mm and 1mm data are shown by filled ellipses at the bottom right corner of the figure.

Assuming standard LTE conditions, the observed $H^{13}CO^+$ emission can be used to compute the column densities and enclosed mass. If we assume a dipole moment of μ=4.08 debye (Haese & Woods1979) and an $H^{13}CO^+/H_2$ ratio of 3.3×10^{-11} (Blake et al. 1987; in OMC1), the observed fluxes indicate an enclosed mass of ∼280$M_\odot$-330$M_\odot$for temperatures of 40 K-50 K. The estimated mass can be uncertain by a few hundred solar masses depending on the assumed value of $H^{13}CO^+/H_2$ ratio and excitation temperature. In any case, the estimated $H^{13}CO^+$ mass is of the same order than the mass evaluated from the 3 mm continuum emission.

3.3. SiO & CO observations

In Fig. 3 we present the results of the SiO J=2–1 and CO J=2–1 high-resolution observations in all the region around ON 1 including the north zone in which the 1.2 mm emission is significant. The SiO emission is found at velocities of $V_{lsr}\pm$4-5$km\,s^{-1}$, with respect to the systemic velocity, whereas the CO emission appears to extend up to $V_{lsr}\pm12km\,s^{-1}$. The CO J=2–1 data at 1.2 mm is quite poor due to summer weather conditions, but the knots shown in Fig. 3 have high signal to noise ratio (10-15σ). Based on complementary blue and red shifted components we can identify at least four main outflows in the region. However, we caution that these maps do not reveal most of the large scale structures in the region, since we do not have any short spacing data from single dish telescopes included in the maps.

The first outflow is seen close to the central FIR source. The most internal component of this outflow is at PA∼45° in good agreement with the $H^{13}CO^+$ outflow component discussed in Section 3.2. As for the $H^{13}CO^+$ data, the blue-shifted emission is placed at the NE of the source, while the red-shifted emission is placed at the SW. We then believe that the SiO and the $H^{13}CO^+$ high velocity emission is tracing the same compact bipolar outflow which is emerging from the very vicinity of the FIR object.

Most remarkably, the region placed 40″ north from ON 1 FIR appears to be an important center of outflow

activity: a prominent high-velocity SiO feature which is marked as A_{blue} in Fig. 3 stretches approximately 30″ in the north-south direction forming a kind of highly-collimated jet. the red shifted counterpart to this jet-like structure is not so obvious. We think that the bright red knot (A_{red}) on the south can be associated with A_{blue} because both structures are well aligned and because there is no other equally prominent blue component in the region. If these two features A_{red} and A_{blue} were actually part of the same outflow, this would have a total size of at least 1′ or 0.5 pc. We caution however that it is difficult to identify bipolar counterparts at large scale in such complex regions.

A smaller outflow denoted by *B* shows both blue and red shifted lobes and extends to about 25″ in the east-west direction. This flow is traced even by the poor quality CO data appearing as spatially separated blue and red knots. The driving source of this outflow has not been identified neither in the near-infrared nor in the mm-wave observations. The 3σ noise limit of 5 mJy of our 3 mm continuum maps imply a limiting detectable mass of 5-6 $M_\odot$. Therefore this outflow is likely driven by a low mass object.

Finally, a short east-west jet-like feature, denoted by *C*, is emerging from the dense blob of SiO emission surrounding the ON 1 source represents another distinct bipolar outflow. Indeed, this flow is traced more prominently by the symmetrically placed CO knots in an axis that closely matches with the axis of the overall bipolar distribution of near-infrared H_2 emission. It is unclear if this outflow arises from the same object than the dense and compact NE-SW outflow seen in $H^{13}CO^+$ and SiO, and which has been discussed above. Since the FIR object is probably a binary system (Kumar et al. 2003), it may be not surprising to find two different outflows emanating from its vicinity.

It appears anyway that high velocity emission is spread all over the cluster forming molecular cloud. Although our observations indicate the presence of real multiple outflows, it is also likely that some of these outflows have interacted with the surrounding cluster and broken into multiple components. This may be particularly true for the east-west flow which is traced by the CO knots, a faint SiO jet and largely by the NIR H_2 emission.

4. Discussion

ON 1 was described to be a rapidly rotating condensation by ZHRS85 based on NH_3 observations. The higher resolution data presented here along with other dense gas and dust tracing observations indicate that the NH_3 condensation described by ZHRS85 actually corresponds to an outflow. The $H^{13}CO^+$ observations discussed in Section 3.2 has the orientation and velocity ranges similar to the NH_3 features. However, for the first time, our observations shows a spatially resolved bipolar feature whose PV diagram is typical of outflows. Perhaps the $H^{13}CO^+$ observations alone would not have resolved the issue if this is an outflow or a rapidly rotating envelope, particularly because of the velocity structure close to the source and the low values of $\Delta v = V_{lsr} \pm$2-3km s^{-1}. But the SiO emission which traces other outflows in the region show only slightly higher values of $\Delta v = V_{lsr} \pm$4-5km s^{-1}. The symmetrical lobes of $H^{13}CO^+$ emission indicate that the outflow has a small inclination angle with respect to the plane of the sky. This implies small line-of-sight velocities of the $H^{13}CO^+$ structure in comparison to the SiO data. Indeed all other dense gas tracers from this region such as CS (Shirley et al.2003), CH_3CN (Pankonin et al.2001) and HNCO (Zinchenko et al.2000) display similar V_{lsr} ∼11-12km s^{-1}and Δv ∼4-5km s^{-1}. Therefore it is clear that the $H^{13}CO^+$ presented here spatially resolves the NH_3 data from ZHRS85 and reveal an outflow well placed in the plane of the sky and possibly slow moving. A similar example where a large scale coherent NH_3 structure (Jackson et al. 1988) is aligned well with an outflow (Bachiller & Cernicharo 1990) is found in the case of NGC6334I.

In the light of above results, the following scenario appears most plausible for the ON 1 region. The UCHII region ON 1 is a relatively isolated massive star forming region associated with a small embedded cluster, all of which is immersed in a molecular clump of few thousand solar masses. The vicinity of the UCHII region appears to drive at least two (the $H^{13}CO^+$ compact outflow, the flow traced by CO knots and H_2) and likely three (SiO flow A) major outflows indicating multiple embedded sources of similar evolutionary states. While the exact driving sources for each of these flows are not clear, it is very likely that the $H^{13}CO^+$ flow originate from one of the two mid-infrared (10μm) sources (Kumar et al. 2003) centered on ON 1. These two mid-IR sources are neither visible at 3.8μm nor distinguishable by the millimeter observations. However, given that both sources show 10μm emission and are associated with an unresolved mm continuum peak, and likely drive outflows, they may be at a similar evolutionary state. Thus the ON 1 source could harbor a massive binary protostar.

The $H^{13}CO^+$ and SiO outflows display very low line-of sight velocities. Low values of line of sight velocities in outflows can be expected if they lie in the plane of the sky as appears to be case for $H^{13}CO^+$ flow. But the SiO flow does not obviously appear to be oriented in the plane of the sky therefore indicating that the low line of sight velocities are representative of the region. The outflow traced by $H^{13}CO^+$ does not seem to show any obvious SiO counterparts. SiO production requires violent shocks and dust grain destruction while $H^{13}CO^+$ outflow emission only requires the acceleration of the dense core material (commonly traced by $H^{13}CO^+$). Given the high density of the central regions of this symmetric clump, the outflow traced by $H^{13}CO^+$ is likely encountering viscous forces thus only able to accelerate the gas rather than produce violent shocks. Further, since all dense gas tracers also display similar range of low velocities such as the observed outflows, it is suggestive that the outflows are experiencing an opposing force in its passage through the

very dense, cluster forming core. Since the jet/outflow experiences the viscous forces uniformly from the point of ejection, the force only makes the flow have much lower velocities in comparision to other outflows.

The presence of a surrounding embedded cluster to ON 1 UCHII region represents a low mass stellar population that could be anywhere from Class I to pre-main sequence phases. If we consider that low mass stars form in $\sim 10^6$yrs and massive stars form in $\sim 10^5$yrs, the simultaneous presence of two massive outflows and the central location of the luminous sources provide two alternative scenarios. Either the massive star formation began much later than low mass star formation in this cluster forming core or that the formation of massive star/UCHII region phases last for much longer than $\sim 10^5$yrs. While Herbig (1962) suggested that massive stars form *preferentially* late in the evolution of a cluster, Stahler (1985) argued that it is indeed so due to statistical reasons. In a related context, de Pree et al. (1995) suggest that the life times of the UCHII regions can be much longer than a few thousand years if they form and exist in dense and warm environments. The black body fits to the FIR flux densities of several relatively isolated massive star forming regions (ex: Hunter et al.2000; Mueller et al.2000; Beuther et al. 2002) suggest high temperatures between 50-100K and densities $\geq 10^5 \mathrm{cm}^{-3}$ supporting the scenario predicted by de Pree et al. (1995). This is also true for ON 1 in view of the high estimated column densities and temperatures. However these observations can not effectively rule out the possibility that massive star formation initiated much later than the surrounding cluster of low mass stars.

The FIR and radio flux of the ON 1 source and the mass estimates from this work suggest that ON 1 is among the early B type candidate massive protostars. This source can be compared to other well studied massive protostars such as IRAS05358+3843 (Beuther et al. 2002), IRAS18556+0136 (Fuller et al. 2001) or W75N (Shepherd et al. 2003). While W75N and IRAS18566+0136 have UCHII regions, IRAS05358+3843 has none and is likely about the same age as the massive protostars such as IRAS20126+4104 (Cesaroni et al. 1999) and IRAS23385+6053 (Fontani et al.2004). Among all these, ON 1 is a neat example of a circularly symmetric molecular condensation with a centrally placed massive binary protostar which is driving multiple outflows and surrounded by a young stellar cluster.

Acknowledgements. We gratefully acknowledge Roberto Neri and Sebastian Muller for their extremely helpful support during the reduction of the IRAM interferometric data. This work has been supported by grant POCTI/1999/FIS/34549 approved by FCT and POCTI, with funds from the European Community programme FEDER, and by Spanish MEC grant PNAYA2000-0967.

References

Bachiller, R. & Cernicharo, J. 1990, A&A, 239, 276
Blake, G. A., Sutton, E. C., Masson, C. R., & Phillips, T. G. 1987, ApJ, 315, 621
Beuther, H., Schilke, P., Menten, K. M., Motte, F., Sridharan, T. K. & Wyrowski, F. 2002, ApJ, 566, 945
Beuther, H., Schilke, P., Gueth, F., McCaughrean, M., Andersen, M., Sridharan, T. K., & Menten, K. M. 2002, A&A, 387, 931
Cesaroni, R., Felli, M., Jenness, T., Neri, R., Olmi, L., Robberto, M., Testi, L., & Walmsley, M. 1999, A&A, 345, 949
de Pree, C. G., Rodriguez, L. F. & Goss, W. M. 1995, RMxAA, 31, 39
Desmurs, J. F. & Baudry, A. 1998, A&A, 340, 521
Downes, D., Genzel, R., Moran, J. M., et al. 1979, A&A, 79, 23
Downes, D., Radford, S. J. E., Guilloteau, S., Guelin, M., Greve, A. & Morris, D. 1992, A&A, 262,424
Fontani, F., Cesaroni, R., Testi, L., Walmsley, C. M., Molinari, S., Neri, R., Shepherd, D., Brand, J., Palla, F., & Zhang, Q. 2004, A&A, 414, 299
Fuller, G. A., Zijlstra, A. A., & Williams, S. J. 2001, ApJ, 555, L125
Haese, N. N., & Woods, R. C. 1979, Chem. Phys. Lett., 61, 396
Herbig, G. H., 1962, ApJ, 135, 736
Henning, Th., Michel, B., & Stognienko, R. 1995, Planet. Space Sci. (Special issue: Dust, molecules and backgrounds), 43, 1333
Ho, P. T. P., Haschick, A. D., Vogel, S. N., & Wright, M. C. H., 1983, ApJ, 265, 295
Hunter, T. R., Churchwell, E., Watson, C., Cox, P., Benford, D. J. & Roelfsema, P. R. 2000, AJ, 119, 2711
Israel, F. P., & Wootten, H. A. 1983, ApJ, 266, 580
Jackson, J. M., Ho, P. T. P. & Haschick, A. D. 1988, ApJ, 333L, 73
Kumar, M. S. N., Bachiller, R., & Davis, C. J. 2002, ApJ, 576, 313
Kumar, M. S. N., Davis, C. J. & Bachiller, R. 2003, Ap&SS, 287,191
Kurtz, S., Churchwell, E., & Wood, D. O. S. 1994, ApJS, 91, 659
MacLeod, G. C., Scalise, E., Saedt, S., Galt, J. A., & Gaylard, M. J. 1998, AJ, 116, 1897
Menten, K. 1991, ApJ, 380L, 75
Mueller, K. E., Shirley, Y. L., Evans, N. J., II & Jacobson, H. R. 2000, ApJS, 143, 469
Pankonin, V., Churchwell, E., Watson, C. & Bieging, J. H. 2001, ApJ, 558, 194
Shepherd, D., Testi. L., & Stark, D. P. 2003, ApJ, 584, 882
Shirley, Y. L., Evans, N. J., Young, K. E., Knez, C. & Jaffe, D. T. 2003, ApJS, 149, 375
Stahler, S. W., 1985, ApJ, 293, 207
Turner, B. E., & Matthews, H. E., 1984, ApJ, 277, 164
Watson, C., Araya, E., Sewilo, M., Churchwell, E., Hofner, P., & Kurtz, S. 2003, ApJ, 587, 714
Zhang, Q., Hunter, T. R., & Sridharan, T. K., 1998, ApJ, 505, L151
Zheng, X. W., Ho, P. T. P., Reid, M. J., & Schneps, M. H. 1985, ApJ, 293, 522
Zinchenko, I., Henkel, C. & Mao, R. Q. 2000, A&A, 361, 1079